A measurement of the Lorentz angle in silicon strip sensors at cryogenic temperature

I. Johnson, C. Amsler, V. Chiochia, A. Dorokhov, H. Pruys, C. Regenfus, J. Rochet

Physik–Institut der Universität Zürich

Winterthurerstr. 190, CH-8057 Zürich, Switzerland

Abstract

A geometric model of charge collection has been developed to measure the Lorentz angle in silicon sensors. The model relates the track inclination to the average cluster width. A Lorentz angle of $19.6 \pm 0.27\ ^{+1.0}_{-0.5}{}^{\circ}$ was measured by fitting the model to cosmic ray data collected with the double–sided silicon strip sensors of the ATHENA antihydrogen detector. These measurement corresponds to holes drifting in sensors operated at 130 K, in a 3 T magnetic field and with an average internal electric field of 1.3 kV/cm. Comparisons of charge sharing between strips and track residuals for data taken with and without magnetic field are also presented and support this measurement.

Key words: Silicon sensors, micro-strips, Lorentz angle

PACS: 85.30 De, 29.40 Gx, 29.40 Wk

Email address: ian.johnson@cern.ch (I. Johnson).

1 Introduction

Modern physics experiments commonly use precise (<50 μm position resolution) silicon strip and pixel detectors in strong magnetic fields (>1 T). Electrons and holes propagate under the influence of an electric field to the implants where they are collected. In the presence of a magnetic field, the Lorentz force tilts the drift direction with an angle λ and displaces the reconstructed position [1].

The magnitude of the Lorentz angle and the correction to be applied to the reconstructed position can be measured in many different ways [2–4]. In this article we introduce a geometric model that describes the charge spread amongst strips. This model is applicable to both electrons and holes and may be directly applied to data. We have applied the model to cosmic ray data to measure the Lorentz angle for propagating holes in silicon strip sensors. Further crosschecks that investigate charge sharing and track residuals support this measurement. This paper is organized as follows: in section 2 a short description of the model is provided, in section 3 the model is applied to the data and the measurement is described, sections 4 and 5 respectively present the crosschecks of the charge spread and track residuals, and Appendix A contains a detailed derivation of the geometrical model.

2 Charge spread model

Due to the propagation of charge carriers along the Lorentz angle, the charge spread at the collection surface is distorted in length and displaced, as shown in Fig. 1. Tracks that traverse the silicon parallel to the Lorentz deflection

(Fig. 1a) generate the shortest charge spread and have similar charge collection properties to tracks that cross perpendicular to the sensor plane in the absence of a magnetic field. The shift in the mean position of the a cluster is given by

$$\Delta x = \frac{t}{2} \tan \lambda, \tag{1}$$

where t is the depletion depth. The resulting charge spread is given by

$$L_c = t \left| \tan \theta - \tan \lambda \right|, \tag{2}$$

where the angle θ is the inclination of the track in the direction perpendicular to the strips, as shown in Fig. 1. The track length d is given by

$$d = t \sqrt{\tan^2 \theta + \tan^2 \phi + 1}, \tag{3}$$

where the angle ϕ corresponds to the inclination of the track in the direction parallel to the strips. The curvature in the magnetic field has been neglected.

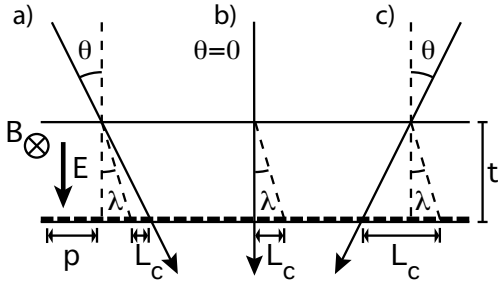

Fig. 1. Cross section of a sensor showing the deflected charge spread L_c for charge carriers (holes) generated along various charged trajectories and that propagate along the Lorentz angle λ. The readout pitch is p.

L_c is related to the measurable quantity $\langle n_s \rangle$, the average number of strips above a given charge threshold. A model of $\langle n_s \rangle$ versus track geometry is derived under the following assumptions: (i) track entry positions are uniformly distributed between readout strips, (ii) the Lorentz deflection is con-

stant throughout the depletion depth, (iii) the charge is linearly shared between adjacent strips, and (iv) the energy loss per unit length μ is constant. Linear charge sharing is a good approximation for silicon micro–strip sensors with floating strips that distribute charge between readout strips. This assumption is motivated and discussed in Sec. 4. In reality, energy loss within the silicon thickness is not constant, but follows a Landau distribution with a long tail towards higher energy depositions. Hence, clusters with similar average energy loss per unit length must be selected from the data in order to better satisfy assumption (iv).

The quantity $\langle n_s \rangle$ is a function of track inclination (θ, ϕ). With these angles, the path length d and the cluster width L_c are known. Furthermore, the total energy deposited μd and $\rho_c = \mu d / L_c$, the energy per unit length along the readout plane, are also known. However, the impact position with respect to strip locations is not required, since $\langle n_s \rangle$ is calculated by averaging the entry positions over one readout pitch. Under the assumption that hit positions are uniformly distributed, the average $\langle n_s \rangle$ is twice the distance x_{th} from the center of a cluster to the position of a readout strip with a charge signal equal to the charge threshold C_{th} divided by the readout pitch:

$$\langle n_s \rangle = \frac{2x_{th}}{p}. \tag{4}$$

The mathematical derivation of x_{th} is given in Appendix A. For a given sensor geometry x_{th} depends only on the Lorentz deflection λ, the track inclination angles θ and ϕ, and the charge threshold C_{th}. Often the Lorentz angle is determined by measuring the angle corresponding to the minimum value of $\langle n_s \rangle$ [2,5]. However, in our model the minimum does not occur for $\theta = \lambda$, but is

offset towards tracks with smaller $|\theta|$ values which produce a smaller number of charge carriers.

3 Lorentz angle measurement

This model has been used to measure the Lorentz deflection in sensors operated at a temperature of 130 K in a 3 T magnetic field. The measurement was performed with cosmic ray data acquired with the detector [6] used by the ATHENA [7,8] antihydrogen experiment at CERN. The micro–strip sensors were produced by SINTEF (Norway) on ≈16 kOhm n–type, $\langle 111 \rangle$ oriented base material of 380 μm thickness. The sensors are 82×19 mm^2. The p–sides of the sensors (collecting holes) are segmented into 384 strips of 46.5 μm pitch with 32 μm implant width and 14.5 μm spacing. Every third strip is metallized to establish an AC–coupling to the readout electronics, while the two inner strips are left floating. The resulting readout pitch is 139.5 μm. The strips are surrounded by a 6 fold progressive multi guard ring structure of the SINTEF type. The n–sides of these sensors are divided into 64 DC coupled pads of 1.25 mm width and 60 μm spacing. These pads are oriented perpendicular to the strips and are individually surrounded by p–stop rings with a guard ring around the border of the sensor. The sensor depletion voltage is approximately 30 V, determined by C–V measurements. However, we operate at a voltage of 65 V to insure good isolation between the n–side structures. This produces an average electric field of about 1.3 kV/cm. A more detail description of the sensors may be found in [6].

The ATHENA detector consists of two concentric cylindrical layers with radii of approximately 4 cm and 5 cm. Each layer contains 16 modules that have an

active length of 16.2 cm. The modules are made of two sensors and readout electronics glued onto a silicon support structure. The central axis is parallel to a homogenous 3 T solenoidal magnetic field. Thus, charge drift in the sensors is perpendicular to the magnetic field. Impact positions for charged particles are reconstructed with a center of gravity algorithm on clusters of charge collected by adjacent strips. Cosmic ray trajectories are then reconstructed from the four 3D points by requiring charged particles to fully traverse both cylinders. The four spatial measurements are fitted with a helix for data acquired with the magnetic field on, and a straight line for data without magnetic field.

To better satisfy the constant energy loss constraint, (iv) in Sec. 2, we select clusters with an average energy loss per unit length within ± 15% of the most probable value (0.60 ADC counts/μm). This range is shown by the shaded region in Fig. 2. In particular, the cut towards high energy loss suppresses clusters that contain higher–energy secondary electrons (δ rays) that artificially elongate clusters.

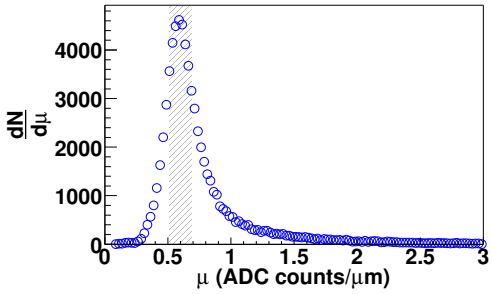

Fig. 2. Distribution of the average energy loss per μm. Clusters in the shaded region were selected for this analysis.

The Lorentz angle was measured by fitting the model to distributions of $\langle n_s \rangle$ as a function of track inclination. The data sample was divided into 21 intervals in ϕ, each of 4° width, and 41 θ bins. Both angles affect the path length and consequently the total deposited energy, while only θ determines

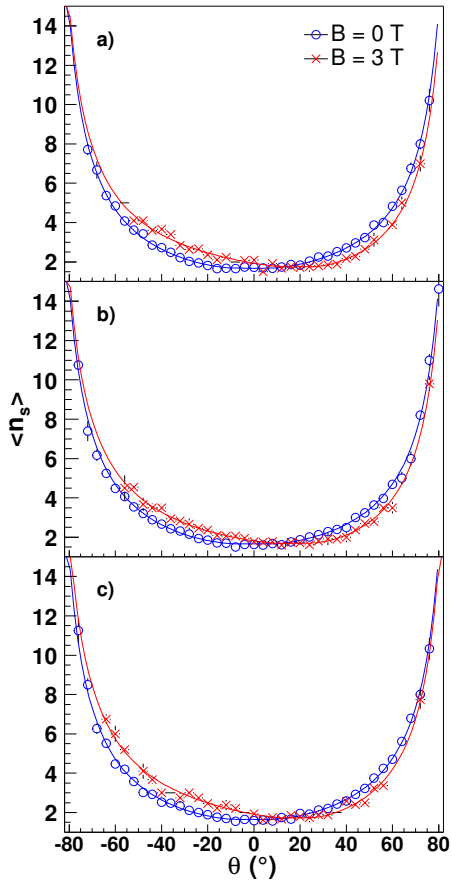

Fig. 3. Distribution of the average number of strips vs. the inclination angle θ in three intervals of ϕ; about ϕ = -20° (a), 0° (b) and 20° (c) for field–off (circles) and field–on (crosses) data. The lines show the fits of the model to the data.

the charge spread across the strips. Equation 4 was fitted to the measured distributions, three of which are shown in Fig 3. As expected, the data taken without magnetic field are symmetric around $\theta = 0$, while data taken with the magnetic field on are shifted towards positive values.

The model describes the data well over its entire range ($-82 < \theta < 82°$ and $-42 < \phi < 42°$). In the fits the readout pitch and μ were fixed to 139.5 μm and 0.60 $\pm$ 0.09 ADC counts/μm, respectively. The remaining parameters (t, C_{th} and λ) were left free in the fits and were later compared with their

expected values. Parameters t and C_{th} extracted from the fits in the various ϕ regions fluctuate statistically about average values. For field–off data the extracted values are $t = 366.5 \pm 1.1$ μm and $C_{th} = 38.6 \pm 0.4$ (stat) $\pm$ 5.8 (syst) ADC counts. For the field–on data the values are $t = 359.9 \pm 2.9$ μm and $C_{th} = 33.3 \pm 0.9$ (stat) $\pm$ 5.0 (syst) ADC counts. These values are fairly close to the nominal values of $t = 380 \pm 15$ μm and $C_{th} = 50$ ADC counts, but are systematically lower than the expected values. We ascribe this systematic offset to the assumption that charge carriers are uniformly generated along trajectories, to the finite range of accepted μ values and to the correlation between them in Eq. A.9. The systematic uncertainty on the Lorentz angle measurement was estimated by repeating the fits with the parameters t and C_{th} varied around their expected values ($350 < t < 400$ μm and $25 < C_{th} < 75$ ADC counts). Variations in the depletion thickness did not introduce a sizable systematic uncertainty, while a systematic uncertainty of $^{+1.0}_{-0.5}{}^{\circ}$ was observed when varying C_{th}.

Fig. 4 shows the extracted values of the Lorentz angle as a function of the impact angle ϕ for data with and without magnetic field. The averages for field–off and field–on are λ = -0.08 $\pm$ 0.12° and 19.6 $\pm$ 0.27 $^{+1.0}_{-0.5}{}^{\circ}$, respectively. As expected the field–off measurement is consistent with zero.

4 Charge sharing

The fraction of the charge collected between the strip with the highest signal and its higher adjacent neighbor is given by

$$\eta = \frac{Q_l}{Q_r + Q_l}, \tag{5}$$

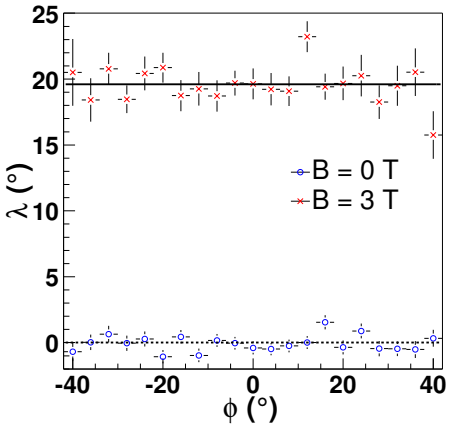

Fig. 4. Distribution of the Lorentz angle λ vs. ϕ for field–off (circles) and field–on (crosses) data.

where Q_l and Q_r are the charge collected by left and right strip. It strongly depends on the charge spread L_c. Tracks traversing the sensor along the Lorentz deflection lead to a small charge spread that is mainly collected by two strips. In this case, the value of η depends on the hit position with respect to the location of the readout strips. The distribution of η for tracks with hit positions uniformly distributed between two strips reveals features of the sensor. For instance, the capacitive coupling between the two inner floating strips and the readout strips is exhibited by the enhancements near $\eta = 0.33$ and $\eta = 0.66$ in Fig. 5a. Two peaks near $\eta = 0.1$ and $\eta = 0.9$ are typically present in data taken without a zero suppressed readout. Our data was taken with zero suppressed readout and strips that collect a small amount of charge were therefore ignored. For this reason we have equally distributed single strip events between the $\eta = 0$ and $\eta = 1.0$ bins in Figure 5.

As the track inclination deviates from the direction of the Lorentz deflection, such that $p/2 < L_c < p$, the smearing of charge smoothes the η distribution (Fig. 5b). For track inclinations that generate a large charge spread ($L_c > 3p$), the inner strips collected a similar amount of charge. Therefore, the η

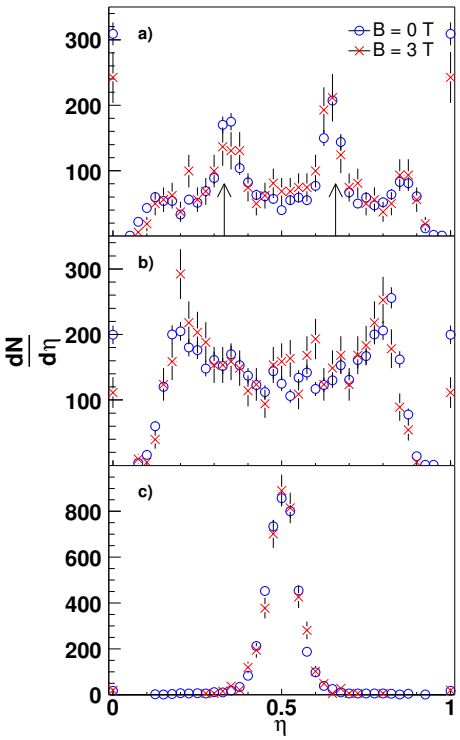

Fig. 5. Distributions of η for field–off (circles) and field–on data (crosses) in the charge spread bins of $L_c < p/4$ (a), $p/2 < L_c < p$ (b) and $3p < L_c < 4p$ (c).

distribution becomes narrow around $\eta = 0.5$ (Fig. 5c).

Since the η distributions strongly depend on L_c, which in turn depends on the Lorentz angle (see Eq. 2), the Lorentz deflection λ can be checked by comparing field–off and field–on distributions. Figure 5 shows comparisons of field–on ($\lambda = 19.6°$) and field–off ($\lambda = 0°$) η distributions in different L_c bins. The observation that the η distributions agree in all L_c bins is a confirmation that the appropriate Lorentz angle has been used in the calculations of L_c.

The interstrip position and the charge sharing function can be obtained using the η distribution for crossing angles almost parallel to the Lorentz deflection ($L_c < 10$ μm, similar to Fig 5a) [9]. For a given η, the distance x between the hit position and a readout strip is given by

$$x = p - \frac{p}{N}\int_0^{\eta} d\eta' \frac{dN}{d\eta'}, \tag{6}$$

under the assumptions that hit positions and detection efficiency are uniform between two readout strip. Where N is the total number of events. The η distribution as a function of x is shown in Fig. 6. This distribution is directly related to the charge sharing function dQ/dx through

$$\eta(x) = \frac{1}{\rho_c}\frac{dQ}{dx}, \tag{7}$$

and is well described by linear charge sharing, a line with a slope of -1.0 and intercept at 1.0. This observation justifies the choice of linear charge sharing in the model (Eq. A.2). The larger deviations from the linear approximation near $x = 0$ and $x = 1$ are caused by the corresponding spikes in the η distribution and are an artifact of the zero suppressed readout.

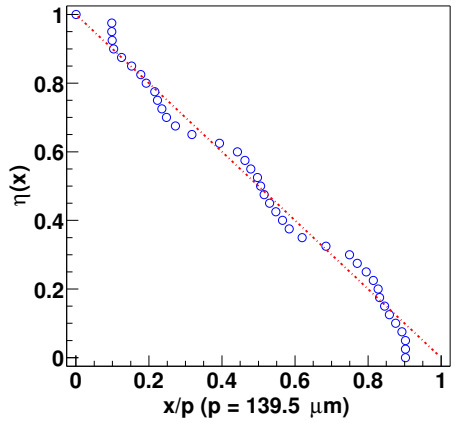

Fig. 6. Distribution of η vs. the interstrip position x.

5 Shift in the measured coordinates

Charge drift along the Lorentz angle translates into a shift in the reconstructed position (Eq. 1). Position shifts are apparent when the reconstructed position

of one of the hits is compared to the position where the helical path of the three remaining hits crosses the sensor. The distribution of this residual, Δs, is shown in Fig. 7. In the ATHENA detector the propagation direction of the holes is inward for the inner layer and outward for the outer layer. Thus resulting in opposing Lorentz angle displacements between the layers that not only shift close hit positions in opposing directions, but also substantially modify the helix parameterization of tracks. The magnified displacement $\Delta s \approx$ 300 μm (uncorrected data in Fig. 7) is much larger than the expected single cluster displacement of $\Delta x = 67.7$ μm for $\lambda = 19.6°$.

To correct for the displacement caused by the drift along the Lorentz angle, all cluster positions were shifted by -67.7 μm along the $\vec{\mathrm{E}} \times \vec{\mathrm{B}}$ direction. The corrected distribution is also shown in Fig. 7. This distribution is in good agreement with the field–off distribution and confirms that the correct Lorentz angle was used to calculate Δx.

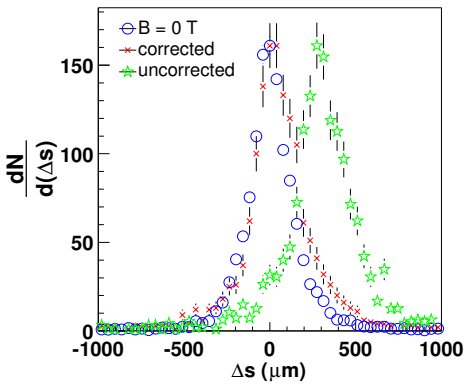

Fig. 7. Distribution of track residuals for field–off data (circles), corrected field–on data (crosses) and uncorrected field–on data (stars).

6 Conclusion

A model relating charge collection in silicon strip sensors to the Lorentz angle has been presented and fitted to data. With this model we have found the Lorentz deflection to be $\lambda = 19.6 \pm 0.27\ ^{+1.0\circ}_{-0.5}$ for propagating holes in silicon strip sensors operating at 130 K, in a 3 T magnetic field and with an average internal field of 1.3 kV/cm. Comparisons of charge sharing and track residual distributions support this measurement. This result is also in good agreement with other low temperature measurements made using a different technique [3].

7 Acknowledgement

We would like to thank R. Brunner, D. Lindelöf and P. Riedler for their contributions to the silicon micro–strip detectors. We also thank G. Ruggiero and M. Swartz for many fruitful discussions.

A Appendix: Derivation of x_{th}

In this appendix the variable x_{th} used in the calculation of $\langle n_s \rangle$ (Eq. 4) is derived. Precisely, x_{th} is the distance between a strip and the center of a cluster when the charge collected by that strip is equal to the charge threshold C_{th}. The charge collected by a strip is given by

$$C = \int_{x_c - L_c/2}^{x_c + L_c/2} dx \frac{dQ}{dx}. \tag{A.1}$$

When linear charge sharing is assumed, dQ/dx is given by

$$\frac{dQ}{dx} = \rho_c \left[\frac{p - |x|}{p}\right] \Theta\left(p - |x|\right). \tag{A.2}$$

$\Theta(y)$ is the unit step function [1]. For our application the linear charge sharing assumption is supported by Fig. 6. The model can also be extended to other charge sharing functions by modifying Eq. A.2.

We define two types of strips within clusters. *Enclosed* strips are at least at a distance p from both ends of the cluster. Hence, all *enclosed* strips mathematically collect the same amount of charge $\rho_c p$. All other strips are considered *edge* strips. Unlike *enclosed* strips, the the amount of charge collected by an *edge* strip depends on the cluster position.

For *edge* strips there are four classes of charge collection integrals (Eq. A.1). The appropriate class for a particular track inclination is determined by comparing the charge width L_c to the minimum charge width m required from an adjacent strip to produce a signal above threshold. For $C_{th} < \rho_c p/2$, m is given by

$$m = \sqrt{\frac{2pC_{th}}{\rho_c}}, \tag{A.3}$$

and for $C_{th} \geq \rho_c p/2$

$$m = 2p - \sqrt{2p^2 - \frac{2pC_{th}}{\rho_c}}. \tag{A.4}$$

These four classes of integrals are sketched in Figure A.1. In class (a) the cluster width L_c is smaller than the pitch and the minimum charge spread m

[1] $\overline{\Theta(y)} = 0$ when $y < 0$ and $\Theta(y) = 1$ when $y > 0$.

(Eq. A.3). Thus, the charge lies between two adjacent strips. In class (b) the charge spread is larger than m (Eq. A.3), but does not surround the strip. So, one end of the charge spread is located at a distance m from an adjacent strip. In these two classes (a) and (b) *edge* strips beyond the edges of L_c may be above threshold. However, for classes (c) and (d) ρ_c is so low that the charge spread must surround *edge* strips for them to be above threshold. In class (c) the charge width L_c is smaller than m (Eq. A.4), therefore neither end of the cluster extends beyond a neighboring strip. In (d) L_c is larger than the minimum charge spread m (Eq. A.4). Thus, one end of the charge spread is a distance m from an adjacent strip and the other extends beyond that neighboring strip.

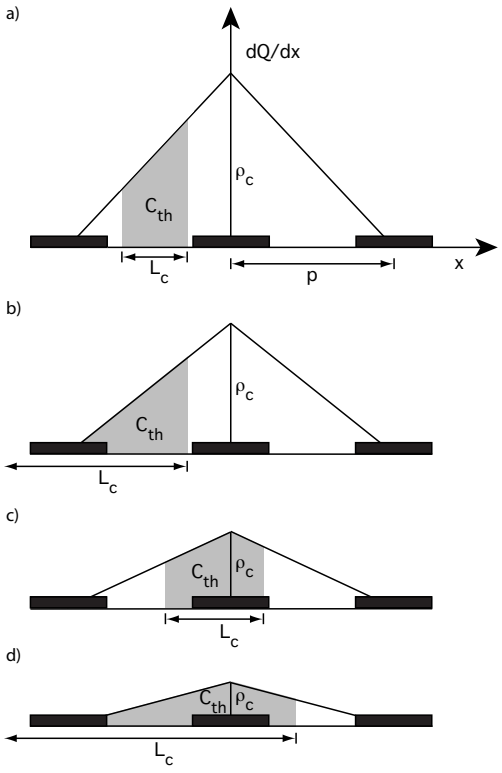

Fig. A.1. Diagrams of the charge collected by a strip when it is at threshold, ordered in decreasing ρ_c.

Detection inefficiencies are dealt with before they enter into the x_{th} calculation.

In cases where, independent of cluster position, the charge density is lower than that required by the charge threshold, x_{th} is set to 0 so that $\langle n_s \rangle = 0$. This occurs when $L_c < 2p$ and

$$C_{th} > \mu d \left(1 - \frac{L_c}{4p}\right), \tag{A.5}$$

or when $L_c \geq 2p$ and

$$C_{th} > \rho_c p. \tag{A.6}$$

In cases where, independent of cluster position, the charge density is sufficient to only produce one strip above threshold, x_{th} is set to $p/2$ so that $\langle n_s \rangle = 1$. This condition occurs when $L_c < p$ and

$$C_{th} > \frac{\mu d}{2}, \tag{A.7}$$

or when $p \leq L_c < 3p$ and

$$C_{th} > \rho_c \left(\frac{3}{4} L_c - \frac{p}{8} - \frac{L_c^2}{8p}\right). \tag{A.8}$$

For all other track geometries $\langle n_s \rangle$ is above 1 and x_{th} is determined by setting the charge C collected by an *edge* strip (see Eq. A.1) equal to the charge threshold C_{th}. For class (a) geometries, where $L_c = 0$ or $L_c < m$, x_{th} is given by

$$x_{th} = p - \frac{C_{th} p}{\mu d}, \tag{A.9}$$

while for classes (b) and (d), where $L_c \geq m$,

$$x_{th} = p + \frac{L_c}{2} - m. \tag{A.10}$$

Note that class (c) geometries are previously handled by Eqs. A.5, A.7 and A.8. Equations A.1 – A.10 only depend on the Lorentz deflection λ, the track inclination angles θ and ϕ, the charge threshold C_{th} and the sensor geometry.

References

[1] R. Turchetta, Nucl. Instr. and Meth. A 335 (1993) 44.

[2] N. Bingefors *et al.*, Nucl. Instr. and Meth. A 328 (1993) 447.

[3] W. de Boer, Nucl. Instr. and Meth. A 461 (2001) 200.

[4] A.Dorokhov *et al.*, Nucl. Instr. and Meth. A 530 (2004) 71.

[5] I. Gorelov, Nucl. Instr. and Meth. A 481 (2002) 204.

[6] C. Regenfus, Nucl. Instr. and Meth. A 501 (2003) 65.

[7] M. Amoretti *et al.*, Nature 419 (2002) 456.

[8] I. Johnson *et al.*, Proceedings of the 8^{th} ICATPP'03 (to be published by World Scientific), physics/0401034.

[9] C. Amsler *et al.*, Nucl. Instr. and Meth. A 480 (2002) 501.